DEVELOPMENT OF METALLIC HOT GAS FILTERS

I. E. Anderson
Metal & Ceramic Sciences Program, Ames Laboratory (USDOE),
Iowa State University, Ames, IA. 50011, USA
E-mail: andersoni@ameslab.gov; Telephone: (515) 294-9791; FAX: (515) 294-8727

B. Gleeson
Metal & Ceramic Sciences Program, Ames Laboratory (USDOE),
Iowa State University, Ames, IA. 50011, USA
E-mail: bgleeson@ameslab.gov; Telephone: (515) 294-5606; FAX: (515) 294-8727

R. L. Terpstra
Metal & Ceramic Sciences Program, Ames Laboratory (USDOE),
Iowa State University, Ames, IA. 50011, USA
E-mail: terpstra@ameslab.gov; Telephone: (515) 294-5747; FAX: (515) 294-8727

ABSTRACT:
Successful development of metallic filters with high temperature oxidation/corrosion resistance for fly ash capture is a key to enabling advanced coal combustion and power generation technologies. Compared to ceramic filters, metallic filters can offer increased resistance to impact and thermal fatigue, greatly improving filter reliability. A beneficial metallic filter structure, composed of a thin-wall (0.5mm) tube with uniform porosity (about 30%), is being developed using a unique spherical powder processing and partial sintering approach, combined with porous sheet rolling and resistance welding. Alloy choices based on modified superalloys, e.g., Ni-16Cr-4.5Al-3Fe (wt.%), are being tested in porous and bulk samples for oxide (typically alumina) scale stability in simulated oxidizing/sulfidizing atmospheres found in PFBC and IGCC systems at temperatures up to 850° C. Recent "hanging o-ring" exposure tests in actual combustion systems at a collaborating DOE site (EERC) have been initiated to study the combined corrosive effects from particulate deposits and hot exhaust gases. New studies are exploring the correlation between sintered microstructure, tensile strength, and permeability of porous sheet samples. Support is gratefully acknowledged from DOE-FE (ARM) through Ames Lab contract No. W-7405-Eng-82.

INTRODUCTION:

The Annual Energy Review 2001, released by the US Department of Energy's Energy Information Administration (EIA), reported that a total of 3,602 billion kilowatts of electricity were consumed in 2001 by the residential, commercial and industrial sectors of the US economy. The review also forecasts that by the year 2020 the demand for electricity could increase by approximately 45% more than the current level. Assuming an average plant size of 300 megawatts, a quick calculation indicates that nearly 1,400 new power-generating plants will need to be constructed to meet the projected demand for electricity.

The EIA report also projects that coal will remain a dominant fuel source for the electricity generated throughout the forecasted period. Advanced coal-fired power generation systems have been developed to meet the continuously increasing demand for electricity in an efficient and environmentally aware manner. These systems are typically based on either pressurized-fluidized bed combustion (PFBC) or integrated gasification combined cycles (IGCC).

Demonstration plants of both systems have been built and evaluated around the world. Compared to conventional coal burning processes, both have demonstrated the ability to achieve higher efficiencies while maintaining very low emission levels. However, both systems rely on delivering particulate-free gas to the downstream system components such as heat exchangers and turbines. Current techniques to remove flue-gas particles include the use of ceramic "candle" filters designed to remove airborne particles 1μm in diameter and larger. Under normal operating conditions, porous rigid ceramic filter elements are periodically back flushed with a pulse of compressed gas to clear trapped "fly ash" particulate to reestablish and maintain extended filtration service. However, studies have shown that the durability of the existing ceramic filters is unacceptably low, and prone to failure when operated in systems that utilize periodic back flushing during operation. Oakey [1] concluded that ceramic filter elements have limitations that are primarily due to their inherent brittleness, long-term microstructural instabilities, and poor thermal fatigue resistance.

Metallic filters based on the Fe_3Al (iron aluminide) intermetallic compound have been developed as an alternative material for the ceramic hot gas filters. Compared to SiC and Al_2O_3 ceramic filter materials, those based on iron aluminide have demonstrated adequate corrosion resistance to the gas environments produced by combustion processes. Unfortunately, the iron aluminides are relatively brittle at ambient temperature and their strength at 850° C is not sufficient to resist creep elongation. The Ni-Cr-Al-Fe filter material developed at Ames Laboratory has been shown to offer significant benefits over both the ceramic and iron aluminide materials [2]. The Ni-Cr-Al-Fe alloy exhibited the ability to maintain a nearly equivalent resistance to corrosion as the iron aluminide in initial simulated PFBC sulfidizing/oxidizing corrosion tests at 850° C for up to 1000 hrs. Also, the 850° C yield strength of the bulk Ni-Cr-Al-Fe material was observed to be at least 4 times that of a bulk iron aluminide casting. Subsequent work at Ames Laboratory has demonstrated that through selective alloy design the bulk corrosion resistance (weight change) of the Ni-Cr-Al-Fe alloy can be improved to become comparable to the corrosion resistance of the commercially available Fe_3Al alloy when tested in a simulated PFBC gas environment [2,3]. This study evaluated the corrosion resistance of selected metal alloys exposed to an oxidizing/sulfidizing gas environment similar to the environment developed during the IGCC combustion process.

RESULTS and DISCUSSION:

CORROSION TESTING:

The IGCC environment is oxidizing to aluminum but not to iron. As a consequence, the environment is categorized as being "reducing". Relative to the high temperature

oxidizing/sulfidizing PFBC environment, the IGCC system produces an aggressive reducing gas environment at a relatively low temperature, permitting test alloys to include chromia-forming alloys. Also included were Ni- and Fe-based alloys modified with Al+Mo and the Ni-Cr-Al-Fe-base alloys that were found earlier to be highly resistant to the higher temperature (850° C) simulated PFBC conditions (2). An iron aluminide (Fe-15.8 wt/o Al-2.2wt/o Cr-0.2wt/o Zr) sample was also tested to provide a baseline for comparison.

A corrosion test, simulating IGCC conditions, was conducted on the alloys listed in Table 1. Prior to testing, each specimen was pre-oxidized in flowing argon ($P_{O_2} \sim 10^{-6}$ atm) gas at 1000°C for 24 hrs. During the experiment, bulk and porous coupon specimens of Ni-Cr-Al-Fe and other alloys were exposed to a simulated IGCC gas environment having an approximate composition (vol.%) of N_2 – 24 CO – 5 CO_2 – 5 H_2O – 14 H_2 – 1.3 CH_4 – 20 ppm H_2S for 1000 hrs. at a test temperature of 650° C. The weight change of each sample was recorded every 250 hrs after being cooled to room temperature to simulate an IGCC system shut down. While at room temperature the samples were repositioned on the sample tray to minimize local furnace variations.

Commercial alloys (wt.%)	Commercial Name	Test Designation	Scale Type
Fe - 15.8Al - 2.2Cr – 0.2Zr		Fe_3Al	alumina
Fe - 22.0Cr - 20Ni - 18Co - 3Mo + (others)	Haynes 556	Fe-Cr-Ni-Co	chromia
Ni - 16Cr - 4.5Al - 3Fe + (others)	Haynes 214	Ni-Cr-Al-Fe	alumina
Ni - 30Co - 28Cr - 3.5Fe - 2.7Si + (others)	Haynes HR-160	Ni-Co-Cr-Fe	chromia
Modified alloys (wt.%)			
Ni - 16Cr - 9.0Al - 3Fe		Ni-Cr-2xAl-Fe	alumina
Ni - 16Cr - 13.5Al - 3Fe		Ni-Cr-3xAl-Fe	alumina
Ni - 16Cr - 9.0Al - 3Fe - 20Mo		Ni-Cr-2xAl-Mo	Al-Mo oxide
Fe - 17.6Mo - 9.4Al		Fe-Mo-Al	Al-Mo oxide

Table 1. Test alloys

An overview of the weight change data for the cast alloys is shown in Figure 1. As can be seen, the weight change experienced by these cast alloys are, for the most part, relatively similar. However, the Fe-Mo-Al and the Ni-Co-Cr-Fe alloys appear to react quite differently to this environment compared to the other cast alloy coupons. During the initial 250 hrs. of testing, the Fe-Mo-Al alloy demonstrated a positive weight change, while the Ni-Co-Cr-Fe alloy demonstrated a negative weight change. The weight change during the remainder of the test for either alloy was apparently small.

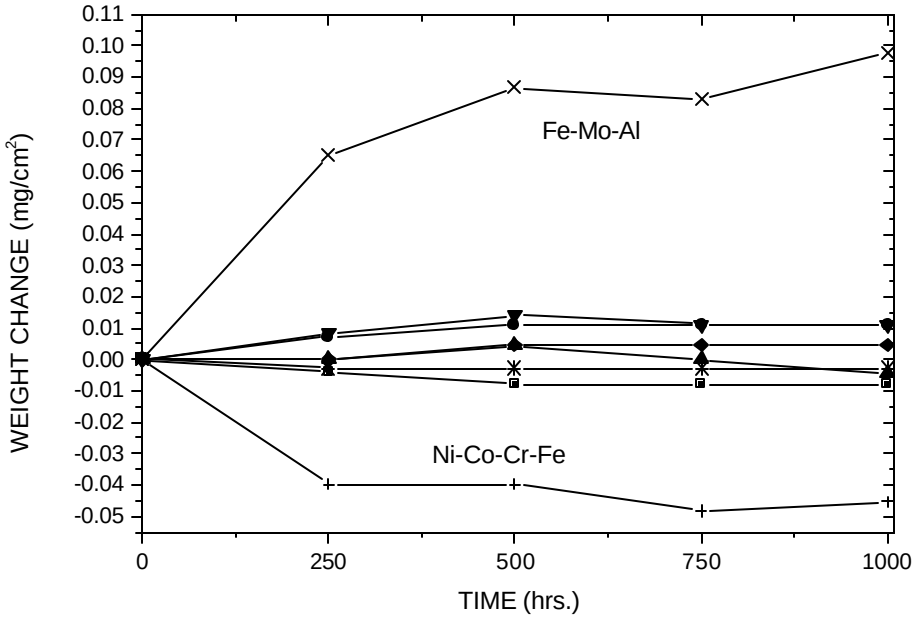

Figure 1. Weight Change of Bulk Alloy Test Sample

Figure 2 shows cross-sectional SEM images of Fe-Mo-Al and Ni-Co-Cr-Fe alloys after exposure for 1000 hrs. The Fe-Mo-Al alloy, with a relatively course two-phase microstructure, formed a very heterogeneous oxide layer, which probably contributed to the significant weight gain indicated in Figure 1. Conversely, the Ni-Co-Cr-Fe sample formed an oxide layer that appeared weak and non-uniformly attached to the sample substrate. As a result, the oxide layer may have spalled from the substrate during sample cooling, resulting in the trend of continuous weight loss indicated in Figure 1.

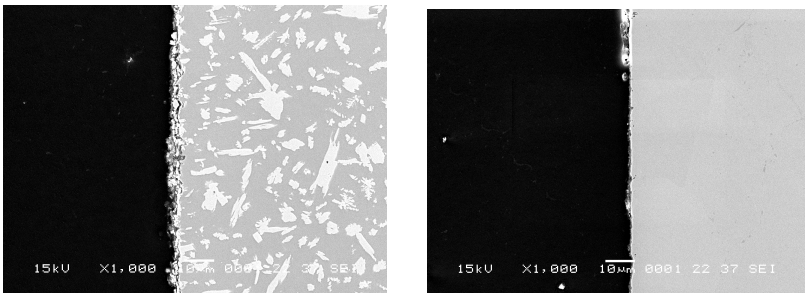

Fe-Mo-Al Ni-Co-Cr-Fe

Figure 2. Cross Sectional SEM Images (1000x)

Figure 3 shows in closer detail the kinetic results of the corrosion test for the remaining bulk alloys. For the alloys in this subgroup, the Fe-Cr-Ni-Co-Mo and the Fe_3Al alloys exhibited the largest weight gain, approximately double that recorded for the Ni-Cr-3xAl-Fe and Ni-Cr-2xAl-Fe alloys, before apparent passivation after 500 hrs. of exposure. As shown in Figure 3, the commercial Ni-Cr-Al-Fe alloy and the Ni-Cr-2xAl-Mo alloys appear to have lost weight in this reducing/sulfidizing gas environment.

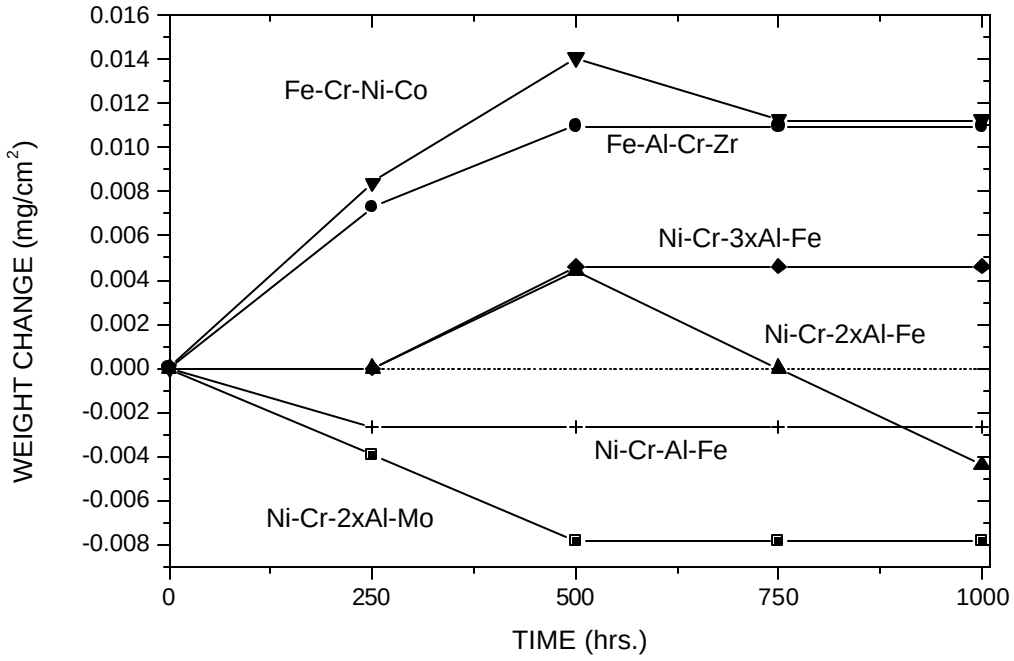

Figure 3. Weight Change of Best Performing Alloys

The cross sectional SEM images of the cast samples, are shown in Figure 4. As can be seen in Figure 4a, the Fe_3Al sample appears to have developed an oxide layer that is relatively thin with a very non-planar, needle-like surface structure. Based on the weight-change results, the oxide layer that formed on the Fe_3Al sample was adherent and resistant to spallation. The Ni-Cr-Al-Fe, shown in Figure 4b, formed the thickest oxide layer, relative to the other samples within this group of alloys. However, the surface of the oxide layer appears to be smoother and absent of the needle-like structure visible in the Fe_3Al image. In agreement with the weight-change data shown in Figure 3, the oxide layer that formed on the Ni-Cr-Al-Fe alloy was reasonably adherent, maintaining a very small, but perceptible weight loss for the full test period.

The scale that formed on the Ni-Cr-2xAl-Fe alloy, shown in Figure 4c, was continuous and nearly the same thickness as the Ni-Cr-Al-Fe alloys. However, there were indications of partial separation at the alloy/scale interface, which is suggested by the mass-loss kinetics after 500 hrs, as seen in Figure 3. The Ni-Cr-3xAl alloy, shown in Figure 4d, formed a very thin oxide layer that, judging from the weight-change kinetics in Figure 3, was relatively adherent. However, the rather discontinuous appearance of the scale suggests that there was partial scale spallation.

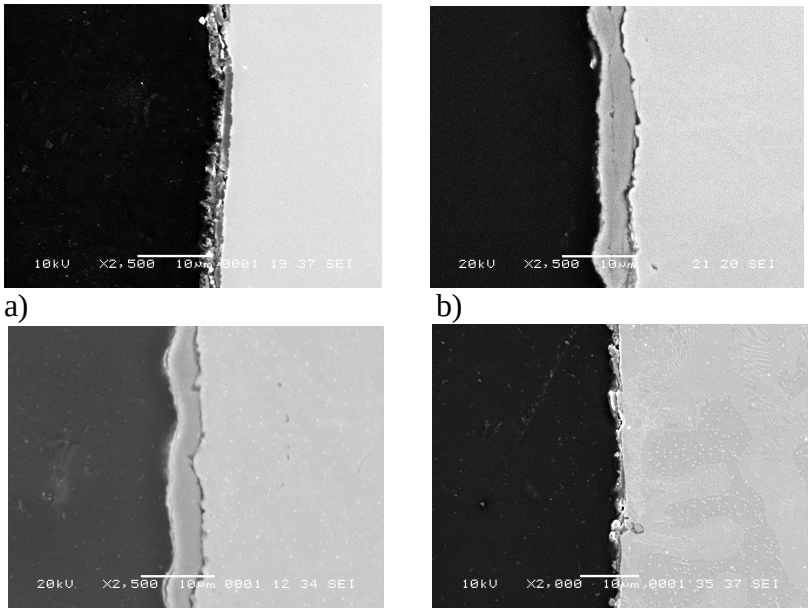

Figure 4. SEM Cross Sectional Images (2500x) of a) Fe_3Al b) Ni-Cr-Al-Fe c) Ni-Cr-2xAl-Fe d)Ni-Cr-3xAl-Fe

The intention of modifying the Ni-Cr-2xAl-Fe alloy with Mo is to confer improved sulfidation resistance in environments that are even more aggressive than that used in this recent test and to improve the alloy's inherent resistance to "down-time" corrosion. This latter type of accelerated degradation is due to the occurrence of acidic HCl condensation on the alloy during service-related cool-down periods. Fe_3Al-based alloys have been reported to be particularly prone to this form of corrosion [4]. Cross-sectional SEM images of the Ni-Cr-2xAl-Fe-Mo alloy, seen in Figure 5, reveal a thin, rather heterogeneous scale layer formed during the test. The scale layer is believed to be a mixture of Al_2O_3 and a metallic Mo-rich phase.

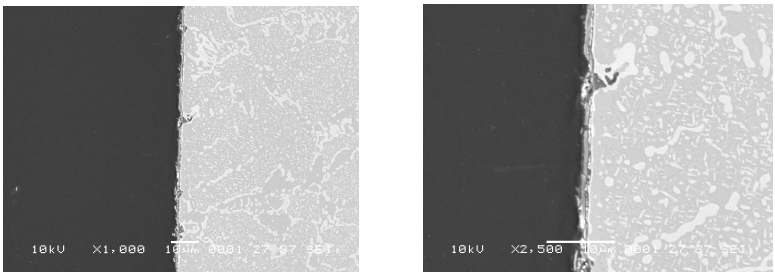

1000x 2500x

Figure 5. Cross Sectional SEM Images of Ni-Cr-2xAl-Fe-Mo Corrosion Test Sample

Figure 6 shows the weight gain per unit area observed (1.3 mg/cm^2, after 1000hrs. testing for a porous sintered sample of Ni-Cr-2xAl-Fe powder relative to the weight change of the cast samples that were tested. As can be seen, the porous sample experienced a significantly larger weight change over the duration of the test in comparison to the cast samples. This apparent accentuation is due to the considerably larger surface area

resulting from the open (porous) sintered microstructure and the fact that only the external surface area of the samples was used to determine the specific weight changes.

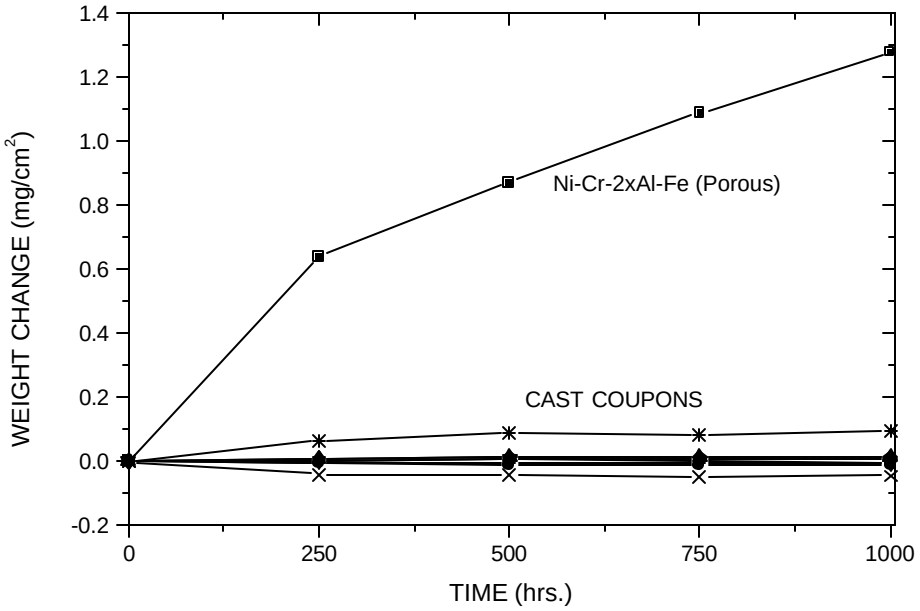

Figure 6. Weight change of Test Samples listed in Table 1

The cross-sectional SEM images in Figure 7 of the porous sintered Ni-Cr-2xAl-Fe powder show that a moderately thin, uniform and continuous oxide layer formed on all of the exposed particle surfaces. The images also indicate that there was virtually no degradation of the partially sintered particle microstructure of the Ni-Cr-2xAl-Fe alloy resulting from exposure to the IGCC gas environment.

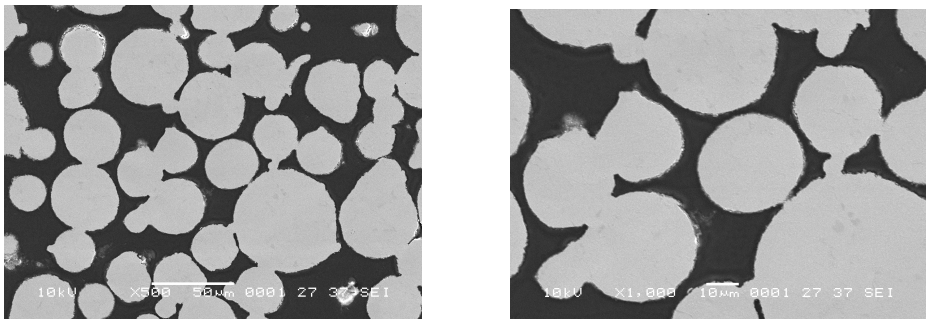

500x 1000x

Figure 7. SEM Images of Porous Ni-Cr-2xAl-Fe

Previous work [2] investigated the corrosion resistance of the Ni-Cr-2xAl-Fe alloy exposed to a simulated oxidizing/sulfidizing gas environment of a pressurized fluidized bed combustion (PFBC) process at 850° C. The results of that investigation indicated that the Ni-Cr-2xAl-Fe alloy performed similar to the Fe_3Al alloy in terms of corrosion resistance. However, a notable improvement in the corrosion resistance over Fe_3Al can be observed when comparing the Ni-Cr-2xAl-Fe alloy exposed to the simulated

environment of the IGCC system used in the present investigation. Future work will investigate corrosion resistance in more aggressive simulated IGCC environments containing up to 2000 ppm H_2S.

As can be seen in Figure 8a, there was an indication in the previous study [2] that the Ni-Cr-2xAl-Fe pre-oxidized alloy particles experienced breakdown in protective scaling behavior after long-term exposure to the simulated PFBC gas environment. This is indicated by the subsurface degradation of the particles, particularly those having a diameter less than 20 µm. Under the PFBC test condition, a porous sintered sample of the Ni-Cr-2xAl-Fe alloy also experienced an enhanced weight change of 4 mg/cm^2, after 1000 hrs. of testing [2]. Conversely, the Ni-Cr-2xAl-Fe alloy exposed to the cooler (650° C) simulated environment of the IGCC system developed an oxide layer only on the particle surface, with no apparent subsurface degradation. As noted above, the weight change at the completion of 1000 hrs. of testing was approximately 1.3 mg/cm^2. These results appear to indicate that the Ni-Cr-2xAl-Fe alloy is a suitable alloy for the IGCC system, with respect to corrosion resistance, but may need more development for use in a PFBC system.

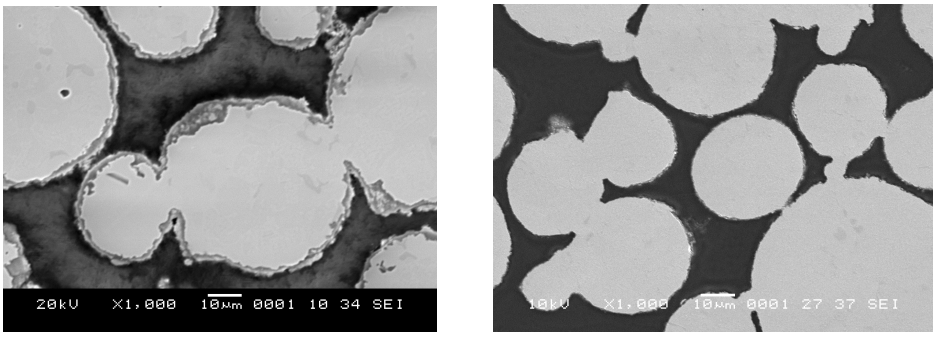

a) b)

Figure 8. SEM Images a) PFBC test conditions b) IGCC test conditions

TENSILE TESTING:

Further porous filter sheet processing developments utilized Ar-atomized Ni-Cr-2xAl-Fe powder and were focused on development of a characterization method that could detect the proper degree of sintered neck evolution for optimum filter sheet properties. Flat tensile specimens from an increasing series of isothermal sintering times were electro-discharge machined (EDM) from porous sheet samples and tensile tested at a strain rate of 0.1mm/sec. The tensile strength was observed to increase at the previously determined optimum sintering time and, then, remain approximately at that peak strength for longer sintering time. The stress-strain curve in Figure 9b shows a smooth elongation trend before ultimate failure is experienced by the sample.

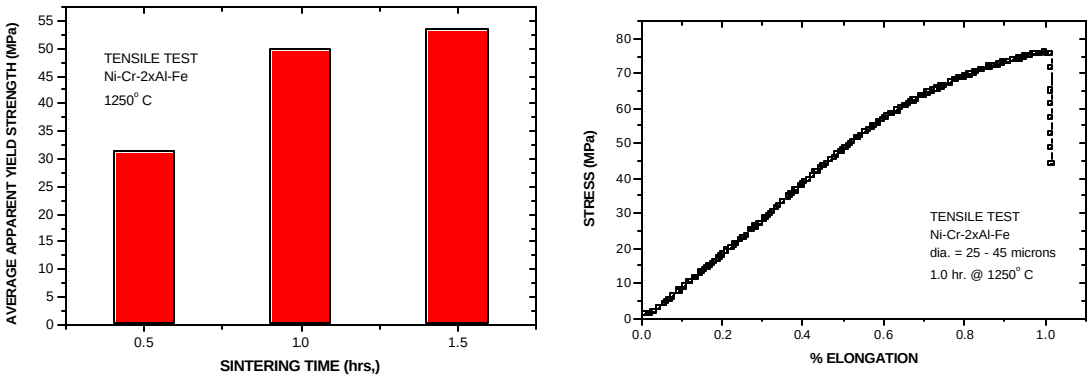

a) b)

Figure 9. a) Average Tensile Test Results b) Tensile Test Stress-Strain Curve

The tensile test samples, sintered for the 3 different sintering times, can be compared in the SEM longitudinal cross-section images shown in Figure 10. As can be seen, the cross-section of the sample sintered for 0.5 hr. appears to be significantly less dense (larger pores and smaller necks) than either of the samples sintered for longer times. Also, only a moderate difference is revealed in the density and porosity of the samples sintered for 1.0 hr. and 1.5 hrs. This observation agrees well with the tensile test results of Figure 9.

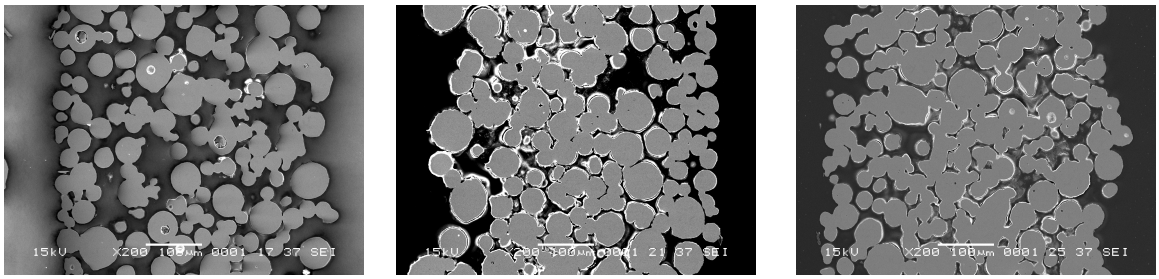

0.5 hr. 1.0 hr. 1.5 hr.

Figure 10. SEM Images (200x) Longitudinal Cross Section

Differences in the etched microstructures of the tensile samples can be seen in Figure 11. There appears to be some level of coarsening of a secondary phase and the grain size when comparing the sample sintered for 0.5 hr. to the samples sintered for 1.0 and 1.5 hrs. The surface of the particles in the sample sintered for 1.5 hrs. appears to have developed a tooth-like feature that is not apparent on the surface of the particles sintered for the shorter periods of time. Apparently, the coarsened secondary phases moved preferentially to the exterior surfaces of the particles after extended sintering. The rough texture, seen on the surfaces of the particle sintered for 1.5 hrs. in Figure 11, is assumed to be the results of the etching treatment attacking the secondary phase that migrated to the periphery of the particle.

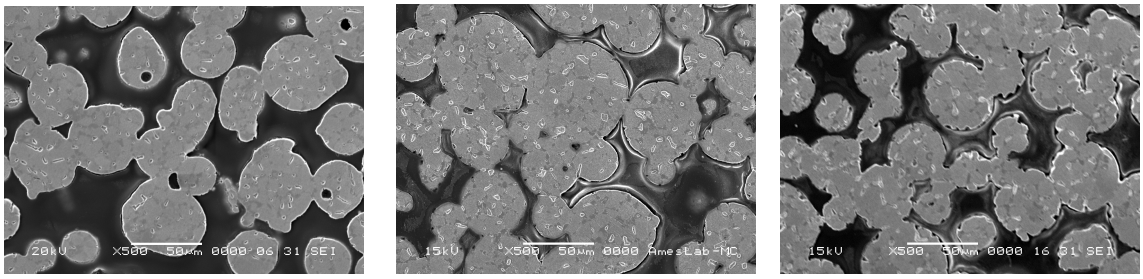

a) 0.5 hr. 1.0 hr. 1.5 hr.

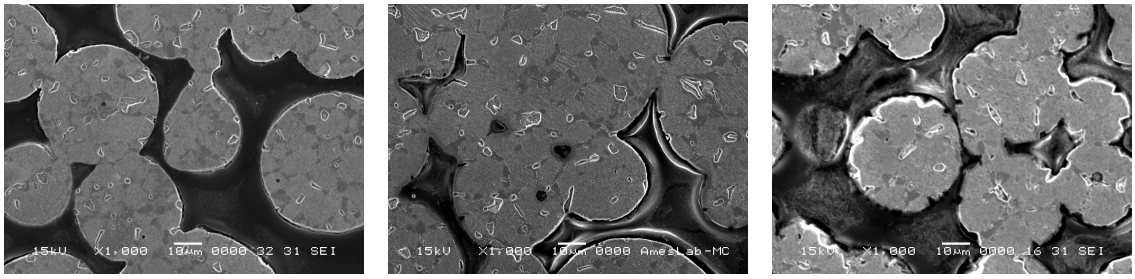

b) 0.5 hr. 1.0 hr. 1.5 hr

Figure 11. SEM Images of Etched Grain Boundaries a) 500x b) 1000x

The fracture surfaces of the tensile test samples shown in Figure 12 also compare well to the strength data reported in Figure 9. As shown, the interparticle bonds form during the 0.5 hr. sintering time are shown to be smaller and less developed than the bonds form during the longer sintering cycle. There appears to be a relationship between the size of the grains developed across each interparticle boundary and the texture of the fracture surface. Further evaluation of this observation is needed.

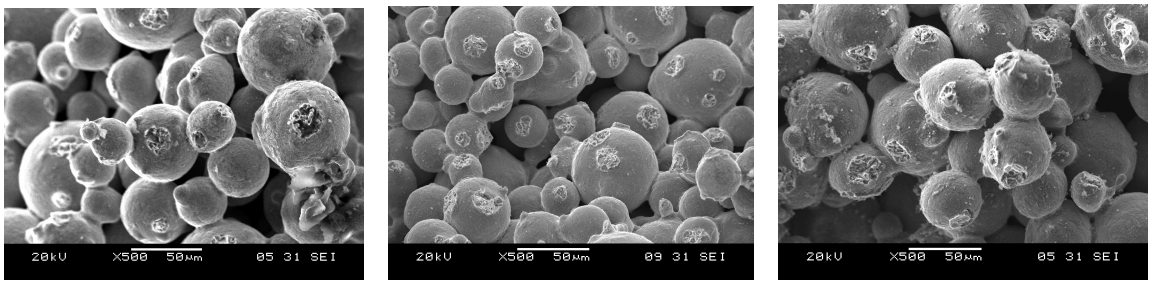

a) 0.5 hr. 1.0 hr. 1.5 hr.

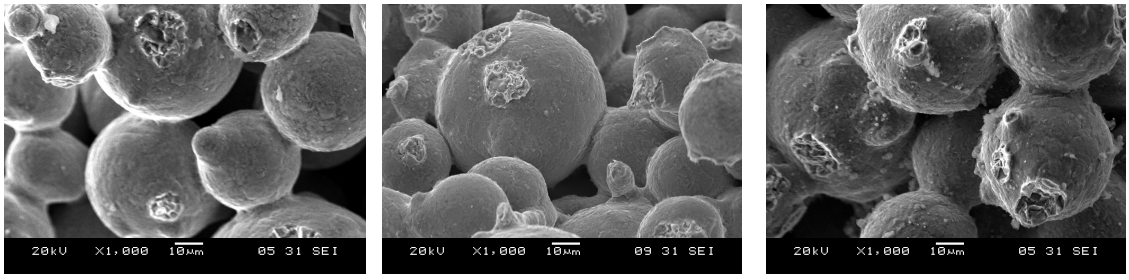

b) 0.5 hr. 1.0 hr. 1.5 hr.

Figure 12. SEM Images of Fracture Surfaces a) 500x b) 1000x

MOLD TESTING:

A search for an alternative mold material was deemed necessary due to long-term problems associated with thermal stress cracking (and industrial handling) of large sheets (about 30cm X 1.5m X 0.5mm in depth) of 96.5% alumina, our current mold choice. As an initial test, a metal mold was fabricated from a piece of wrought Ni-Cr-Al-Fe (50mm x 12.5mm x 10mm) in which a surface cavity (25mm x 10mm x 0.5mm) was machined. The metal mold and cavity were pre-oxidized in air for 100 hrs. at 1000° C to form a protective Al_2O_3 scale layer approximately 1-4 µm thick. After filling the mold cavity with Ni-Cr-2xAl-Fe powder (25 µm > dia. < 45 µm), the powder and mold were processed using a typical (0.2 hrs. at 1250° C) sintering cycle. Unfortunately, the powder apparently reacted with the metal mold material during sintering to a level that prohibited removal of the sintered sample from the mold cavity. Post-sintering observation of the mold surface revealed that the color of the mold had changed from a dull gunstock gray to a reflective silver color. Initially it was thought that the mold was being coated with aluminum which evaporated from the alloy powder when exposed to the high temperature and high vacuum levels of the sintering cycle and, then, condensed on the mold surfaces. To test this assumption, a sample of the mold was characterized using Auger analysis. Figure 13a shows the locations where the Auger depth profiles were conducted on the mold surface, while Figure 13b shows the data collected from spot #1. As can be seen, the mold surface was enriched with nickel, not aluminum. Further testing, also indicated that the nickel was not only evolving from the powder but also the metal mold itself. These results indicated that the pre-oxidation treatment used was not sufficient to prevent powder interactions and that a Ni evaporation/redeposition reaction occurred under vacuum conditions over a range of sintering temperatures (1100 to 1250° C). The most promising results were obtained after plasma spray coating of a Ni-Cr-Al-Fe mold with a continuous, adherent ZrO_2 layer, but further tests must establish the durability and large-scale application ability of this approach.

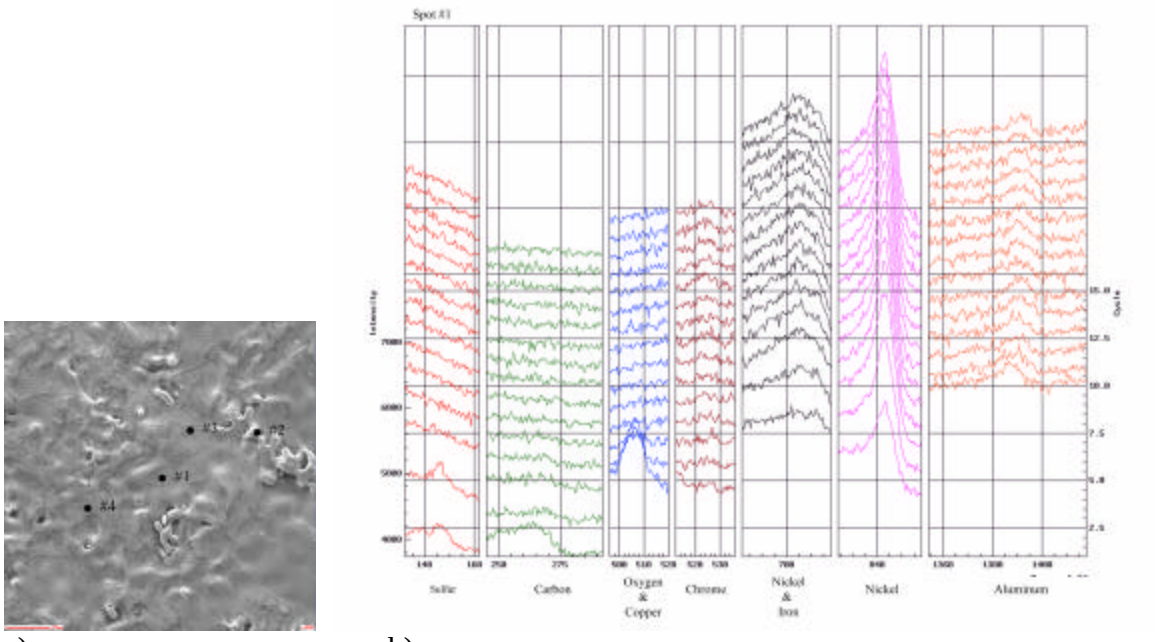

a) b)

Figure 13. a) Auger map b) Auger data

CONCLUSIONS:

In agreement with the weight-change kinetics, surface and cross-sectional characterizations showed that the Ni-Cr-Al-Fe-base alloys were comparable to the iron aluminide after 1,000 hrs. of sulfidation-oxidation testing at 650 °C. The novel Mo-modified Ni-Cr-2×Al-Fe alloy also performed quite well in this simulated IGCC gas environment. In addition to the bulk cast alloys, a porous sample of Ni-Cr-2×Al-Fe alloy also exhibited excellent sulfidation-oxidation resistance, forming a continuous and uniformly thin alumina scale on the exposed (particle) surfaces**.** Interestingly, the same alloy had the best behavior in a previous series of simulated PFBC tests. Tensile testing of thin porous sheet samples proved helpful for assessment of suitable sintering conditions, along with permeability testing. Microstructural analysis of the tensile samples suggested a preferred combination of grain growth and second phase coarsening for an optimum sintered condition. This type of analysis will aid in the development of a full-scale manufacturing process for filter sheets. Additional development of sintering mold material is needed before large porous sheets can be processed.

REFERENCES:

1. Oakey, J.E., Lowe. T., Morrel, R., Byrne, W. P., Brown, R., and Stringer J., Materials at High Temperatures, 14, (1997) p. 301.

2. Terpstra, R. L., Anderson, I. E., B. Gleeson (2002), "Development of Metallic Hot Gas Filters," in Advances in Powder Metallurgy and Particulate Materials, MPIF-APMI, Princeton, NJ, Vol. 1, (2002) p. 92.

3. Terpstra, R. L., Anderson, I. E., B. Gleeson (2001), "Development of Metallic Hot Gas Filters," in Advances in Powder Metallurgy and Particulate Materials, MPIF-APMI, Princeton, NJ, Vol. 8, (2001) p. 84.

4. Bakker, W. T. (1995) *Mixed Oxidant Corrosion in Nonequilibrium Syngas at 540° C*, EPRI TR-104228].

5. Gleeson, B., "High-Temperature Corrosion of Metallic Alloys and Coatings," in Corrosion and Environmental Degradation, Vol. II: Volume 19 of the Materials Science and Technology Series, ed. M. Schutze (Weinheim, Germany: Wiley-VCH), (2000) p. 173.

6. I.E. Anderson, B.K. Lograsso, R.L. Terpstra, B. Gleeson, Powder Metallurgy and Particulate Materials for Industrial Applications, TMS, 2000, p. 11.

7.. Oakey, J.E., Lowe, T., Morrel, R., Stringer, J., and Brown, R., in Proc. 2nd International Conference on Heat-Resistance Materials, K. Natesan, et al. (eds.), ASM International, Materials Park, OH, (1995) p. 537.

8. Alvan, M. A., in Proc. 2nd International Conference on Heat-Resistant Materials, K. Natesan, et al. (eds.), ASM International, Materials Park, OH, (1995) p. 525.